UCRL 86722
WM REC
NTS #

Laboratory measurements of ultralow permeability of geologic materials

D. Trimmer

Earth Science Division, University of California, Lawrence Livermore National Laboratory, Livermore, California 94550

(Received 15 March 1982; accepted for publication 16 April 1982)

A new apparatus is described for determining permeability (water) in geologic materials as a function of confining pressure (to 200 MPa), pore pressure (to 25 MPa), and deviatoric stress (500–800 MPa). The samples are relatively large (0.15 m diameter ×0.28 m long) and may be intact or contain a single through-going fracture. Permeabilities of 10^{-11}–10^{-24} m^2 (10–10^{-12} D) may be measured, simultaneously, with electrical conductivity and acoustic velocity and amplitude. Crack closure is also monitored for the fractured samples. All experimental control and data-acquistion functions are performd by a microcomputer. A discussion of data-analysis techniques and typical data are also presented.

PACS numbers: 91.60. — x, 06.70.Ep

HYDROLOGY DOCUMENT NUMBER 111

INTRODUCTION

The safe terminal storage of high-level radioactive wastes requires that they be isolated from the biosphere for 10^3 to 10^6 yrs, depending upon waste form. One promising method of accomplishing this goal involves placing the wastes underground in stable rock formations. The suitability of such a geological repository depends in part on the fluid transport properties of the surrounding rock, since water transport of dissolved toxic isotopes through rock fractures represents one of the most probable escape paths.

We describe here a new apparatus capable of measuring permeabilities two to three orders of magnitude lower than have been reported by other investigators. The measurements are made on large samples (0.15 m diameter × 0.28 m long) at those confining pressures, pore-water pressures, and differential stresses which encompass the range of expected conditions near a repository constructed to depths of 2 km. Simultaneously, we determine electrical conductance and compressional wave velocity and amplitude. The determination of a relationship between permeability and velocity, amplitude, and conductance may be useful in the nondestructive exploration of potential repository sites, in the monitoring of repository performance after construction, and in the surveillance of the repository area after emplacement of the waste.

I. TESTING TECHNIQUES AND DATA ANALYSIS

Figure 1(a) is a schematic diagram of the 0.15-m-diam by 0.28-m-long test sample. The parameters to be controlled and the measurements to be performed are indicated. The sample may be intact or may contain an induced through-going tensile fracture parallel to the sample axis. The sample is first encapsulated using a thin (0.3 mm) lead jacket and stainless-steel end plates [see Fig. 1(c)]. The jacketed sample is then placed in a pressure vessel and subjected to confining pressures up to 200 MPa. An additional load may be applied in the axial direction which may range up to the failure stress. Pore pressure (usually water) is supplied through the sample end plates at values up to that of the confining pressure. Permeability, conductance, compressional wave velocities and amplitudes, and sample strains are measured simultaneously. If the test sample contains a tensile fracture, the displacement of that surface is also measured. All tests are performed at ambient temperature.

The permeability is determined by inducing a pore water pressure gradient across the ends of the sample and monitoring the subsequent water transport through the sample. The specific technique for determining sample permeability depends upon the value of permeability.

Permeabilities as low as 10^{-17} m^2 (10^{-5} D) are determined with a conventional steady-state flow technique. After a constant flow rate is established through the sample [see Figs. 1(a) and 1(c)], the flow rate through and pressure drop across the sample are measured. Darcy's Law is assumed to be valid, and sample permeability is

$$k = Q\mu L/A\Delta P_s, \qquad (1)$$

where k is the permeability, Q is the volume flow rate, μ is the viscosity of water, L and A are the length and cross-sectional area of the sample, and ΔP_s is the pressure difference maintained across the ends of the sample.

For samples having permeabilities less than 10^{-17} m^2, the water flow rates are too small for convenient direct measurement. Therefore, a transient pulse technique is used for rock samples having permeabilities between 10^{-17} and 10^{-24} m^2. Reservoirs of known volume are introduced upstream and downstream from the sample [see Fig. 2(a)]. The reservoir-sample system is brought to equilibrium at some pore pressure (P_0) [see Fig. 2(b), top left]. At the same time, measurement is initiated by

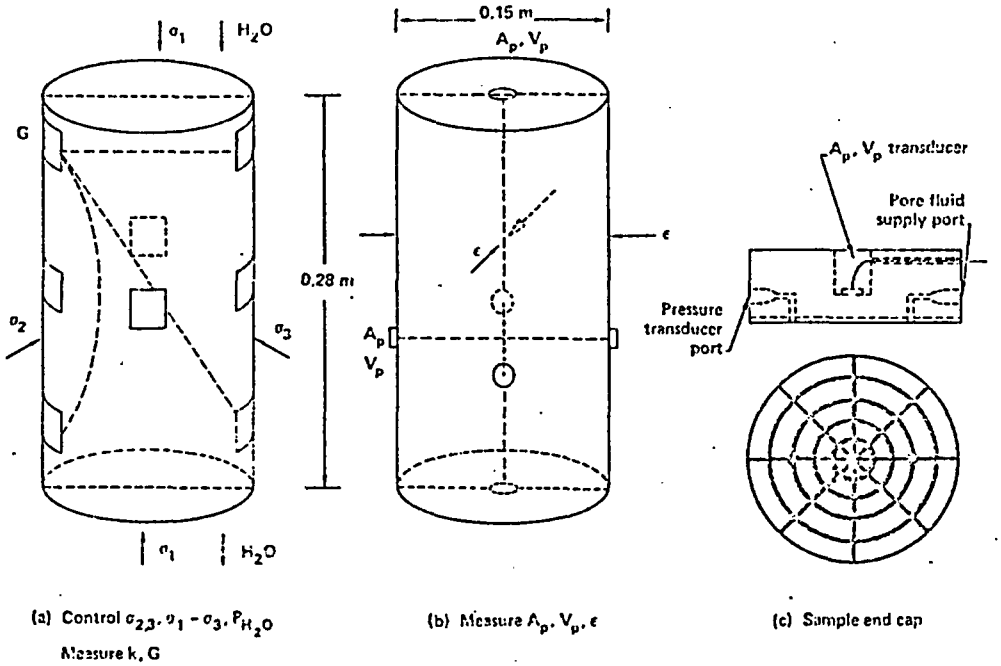

FIG. 1. Schematic of test samples and sample end caps showing applied loads and measurements. The dotted lines show the crack orientation for the fractured samples.

introducing a step increase in pressure (ΔP = 2.0 MPa) into the upstream reservoir [see Fig. 2(b), lower left]. As the pressure pulse travels from the upstream reservoir through the sample and then into the downstream reservoir [see Fig. 2(b), upper right], the pressure-time histories of the upstream and downstream reservoirs are recorded. Measurement is terminated when equilibrium (P_0) has again been reached in the reservoir-sample-reservoir system [see Fig. 2(b), lower right].

For determination of permeabilities in the range 10^{-22}–10^{-24} m^2, the transient pulse technique described above is used with a slight modification. With these extremely low sample permeabilities, the time constant of the system is far too long to wait for equilibrium to be established (2 weeks to 6 months). Therefore, the system is assumed to be in equilibrium when the pressure in the upstream reservoir has changed less than 0.1 MPa in 10^6 s (~1 week). Similarly, measurement is terminated when either the pressure in the upstream reservoir has decayed by 1.0 MPa (50% of the pressure step) or the time has exceeded 10^6 s. The nonequilibrated state of the sample prior to measurement introduces an error of 10% or less (0.1 in 1.0 MPa) in the pressure-time data and a correspondingly small error in the permeability determination.

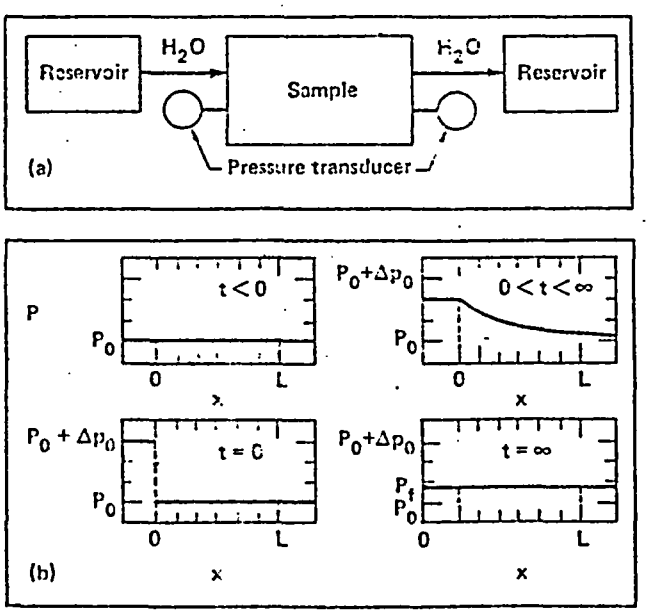

FIG. 2. Schematic of transient pulse technique. (a) Schematic of sample-reservoir system for determining permeability. (b) Pressure profiles across sample-reservoir system with time.

The equation describing the pressure-time history for water flow through a compressible sample-reservoir system is

$$\frac{\partial^2 P}{\partial x^2} = \frac{\mu\beta\phi_c}{k}\frac{\partial P}{\partial t}, \qquad \phi_e = \phi_c + \frac{\beta_r - (1+\phi_c)\beta_s}{\beta}, \tag{2}$$

for $t > 0$, $0 < x < L$, and with boundary conditions

$$\frac{\partial P}{\partial x} = \frac{\mu V_1 \beta}{Ak}\frac{\partial P}{\partial t} \quad x = 0,\ t > 0,$$

$$\frac{\partial P}{\partial x} = \frac{\mu V_2 \beta}{Ak}\frac{\partial P}{\partial t} \quad x = L,\ t > 0,$$

and initial conditions

$$P(x, 0) = P_0 \quad 0 < x \le L,$$

$$P(0, 0) = P_0 + \Delta P,$$

where

P = pressure,
x = distance from the upstream end of the sample,
ϕ_e = the effective sample porosity,
ϕ_c = the interconnected porosity of the sample,

β = the compressibility of water,
S and β_s = the compressibilities of the sample (bulk and mineral matrix, respectively),
V_1 and V_2 = the volumes of the upstream and downstream reservoirs, respectively,
ΔP = the step increase in pressure, and
t = the time since ΔP was applied.

The effective sample porosity is related to the net water storage in the sample during measurement. In previous work,[1] an identical treatment was used. Because the sample was small, however, pore volume was small compared to the reservoir volumes. Therefore, the water storage approached zero and Eq. (2) reduced to

$$\frac{\partial^2 P}{\partial x^2} = 0.$$

When solved with appropriate boundary conditions, this yields

$$k = C - \frac{\mu\beta L V_1 V_2}{A(V_1 + V_2)} \frac{\ln(P_1 - P_f)}{t}, \qquad (3)$$

where C is a constant of integration and P_1 is the pressure in the upstream reservoir.[1] The permeability of a sample can then be determined from the slope of a plot of $\ln(P_1 - P_f)$ vs t, because the rest of the terms are known constants.

Trimmer[2] established that, for this approximation to be valid, the effective pore-volume to reservoir-volume ratio must be less than 0.25. The samples tested in this apparatus are ~600 times larger than those used by Brace *et al.*[1] and have effective pore-volume to reservoir-volume ratios of ~10. The larger sample size facilitates the compressional velocity and amplitude measurements and allows representative samples of large-grained rocks to be prepared. However, the large samples have pore volumes that are not small compared to the reservoir volume. Therefore, the water storage in the rock is significant, and Eq. (2) cannot be simplified. An analytical solution for Eq. (2) and its boundary and initial conditions were only recently found,[4] so the experiment was modeled using a finite-element computer code (see Appendix A).

A parameter study indicated that for a given sample geometry, pore fluid, and reservoir volume, the pressure-time history was a function of permeability and effective porosity. Therefore, if the effective porosity of a sample is known, permeability can be inferred by visually comparing experimental pressure-time histories with numerically generated histories.

There is too much uncertainty in the reported values of β, β_s, and ϕ; thus, these values are not useful in determining the effective porosity. For those samples with time constants small enough to allow sample equilibrium, the effective porosity was determined from the reservoir volumes, P_0, ΔP, and P_f:

$$(P_0 + \Delta P)V_1 + P_0(V_2 + AL\phi_e) = P_f(V_1 + V_2 + AL\phi_e)$$

or

$$\phi_e = \frac{(P_0 + \Delta P - P_f)V_1 + (P_0 - P_f)V_2}{(P_f - P_0)AL}. \qquad (4)$$

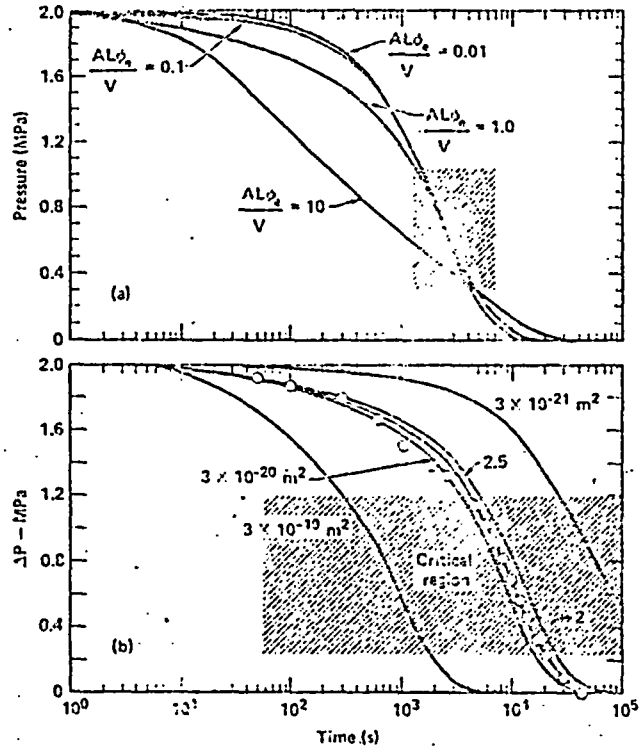

FIG. 3. Numerically generated pressure vs log time histories. (a) Effect of effective pore volume on pressure time histories. (b) Effect of permeability on pressure time histories. Typical data for Westerly granite are shown.

For samples having time constants too long to allow ϕ_e to be determined from Eq. (4), ϕ_e must be determined by comparing the experimental data with the numerically generated curves. The pressure-time histories in Fig. 3(a) were generated using a single permeability value and various effective porosities. Figure 3(b) shows the effect of varying the permeability while holding the effective porosity constant. The open circles are typical data for Westerly granite at 17.5 MPa effective pressure.[3] The effective porosity determines the shape of the curve, while the permeability determines its displacement along the time axis. Therefore, the effective porosity may be determined by comparing the experimental curves to a family of numerically generated curves similar to those in Fig. 3(a).

Once the effective porosity has been determined, a family of curves with the appropriate effective porosity and various permeabilities is generated. The permeability is then inferred by visually matching the experimental data to the numerically generated pressure-time histories [see Fig. 3(b)]. The shaded portion of the curves is given the most weight in determining permeabilities for the following reasons: (1) The thermal transient induced by the initial pressure pulse has disappeared by this time. (2) The slope is greatest, allowing maximum resolution. (3) This portion of the curve is relatively insensitive to the water-storage term [see Fig. 3(a)].

The steepness of the slope and, therefore, the resolution are also increased by using a linear-log plot and by plotting differential pressure versus time. Plotting the differential pressure rather than the upstream pressure also

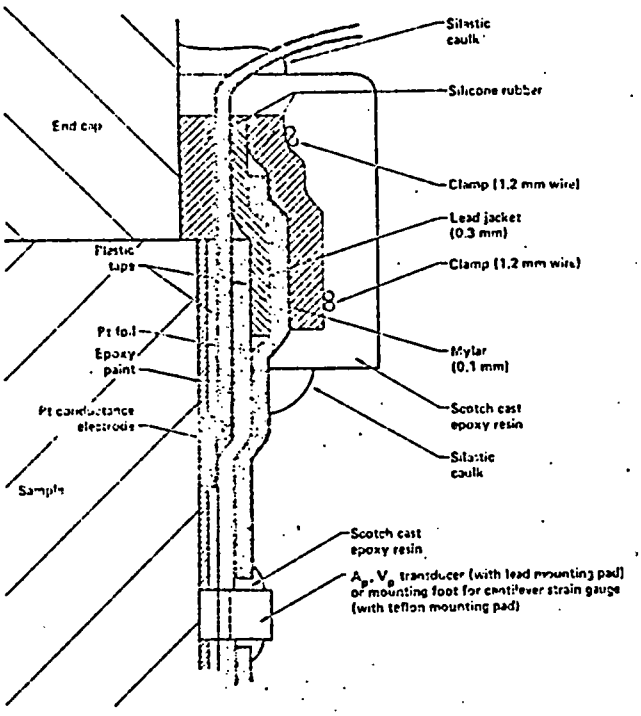

FIG. 4. Schematic of sample jacketing technique for mounting conductance, strain, velocity, and amplitude transducers, and insulating the sample and electrical leads is also diagrammed.

reduces the effects of diurnal temperature variation on the experimental data. If the upstream and downstream reservoirs experience the same thermal history, then a point by point subtraction reduces the thermally induced pressure variations in the data.

It is necessary to generate only one pressure-time history with the appropriate effective porosity, sample and reservoir geometries, and pore fluid parameters. Since the permeability affects only the displacement of the curve along the time axis, the time domain data can be manipulated to produce the pressure-time histories for other permeability values. If $P' = f(t)$ is the pressure-time history associated with permeability, k_0, then $P = f(kt/k_0)$ is the pressure-time history associated with permeability, k.

Pairs of ultrasonic transducers give the change in travel time and amplitude for compressional waves [see Fig. 1(b)]. The pairs are located orthogonal to one another and external to the lead jacket. The conductance, G, of the unfractured sample is measured with a pattern of electrodes on the rock surface; i.e., inside but isolated from the jacket [see Fig. 1(a)]. The ultrasonic and conductance techniques are discussed by Bonner and Schock,[5] Lytle *et al.*,[6] and Trimmer *et al.*[3] Radial sample displacements are monitored to ±6 μm with a strain gauge beam system.[7]

II. SAMPLE PREPARATION

Test samples are prepared from diamond drill core approximately 0.17 m diameter. After diamond grinding the diameter to 0.15 m, the ends are cut and ground to form right circular cylinders 0.28 m long [see Figs. 1(a) and 1(b)]. The transducer locations are masked and the outer diameter of the sample is painted with a marine epoxy paint (see Fig. 4). The masking material then is removed and the conductance electrodes, acoustic transducer, and strain gauge beam mounting pads are positioned. The conductance electrodes (25 mm × 25 mm platinum foil) are placed directly on the sample. The acoustic transducer and the strain gauge beam mounting pads are lead and teflon, respectively, and are cut to fit the sample curvature. The lead pad is cemented to the sample jacket with conductive epoxy, while the teflon pad is placed directly on the sample.

The outer diameter of the sample then is covered with a layer of plastic tape, and windows are cut to expose the transducers and transducer mounting pads. Strips of platinum foil are soldered to the platinum electrodes and laid on the taped surface. The platinum foil then is covered with a layer of plastic tape. The plastic tape serves to prevent fluid flow at the sample-jacket interface, and to electrically isolate the conductance electrode leads from the sample.

The stainless-steel sample end caps [see Figs. 1(c) and 4] are then placed on the sample, and a layer of silicone rubber is used to isolate the conductance leads from the sample end caps. A piece of 0.1-mm Mylar is used to prevent the confining pressure from shearing the electrode leads at the sample end-cap interface.

A piece of 0.3-mm lead sheet is cut approximately 0.30 m × 0.47 m, with windows cut for the beam strain gauge mounting pads. The lead sheet then is wrapped around

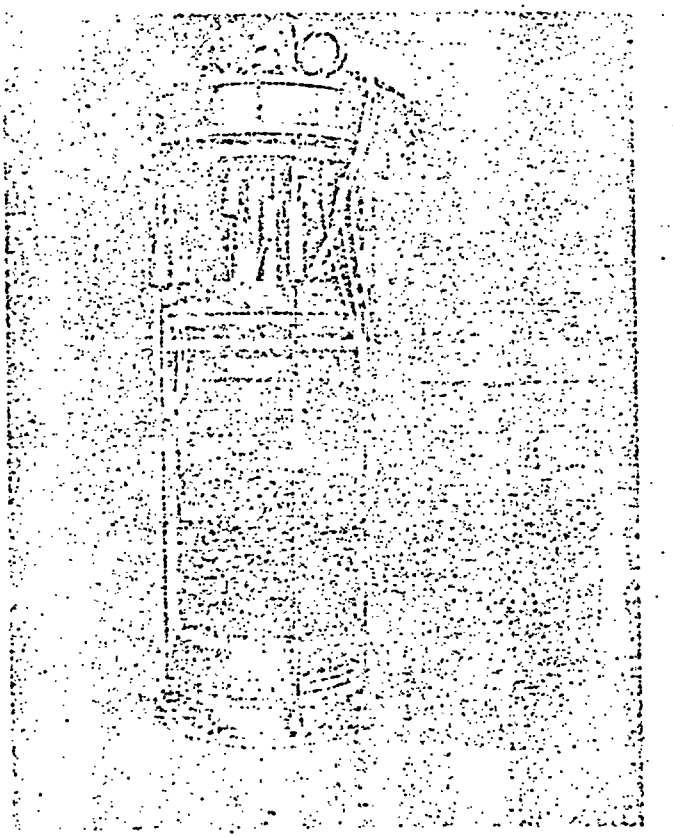

FIG. 5. Sample assembly for intact sample. To the right is a typical sample (White Lake gneissic granite).

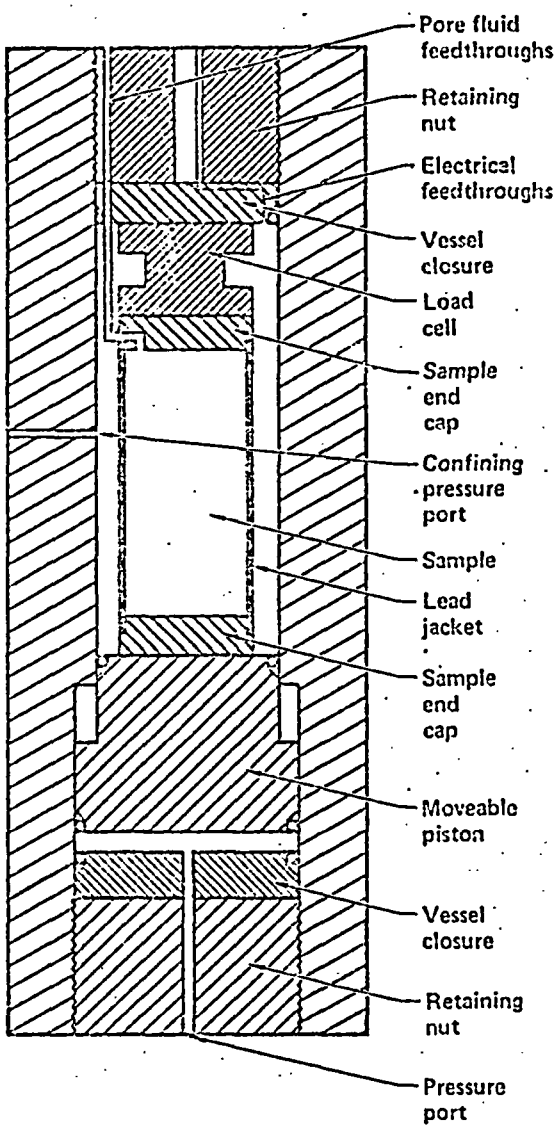

FIG. 6. Schematic of the pressure vessel. The sample assembly and vessel closure are shown. The moveable piston for application of axial loads is also shown at the bottom.

the sample, and the seam is soldered. Another layer of silicone rubber is clamped over the sample-end interface, and the interface region is potted in a flexible epoxy resin. The acoustic transducers are cemented to the lead mounting pads with a conductive epoxy resin, and the strain gauge beam mounting feet are placed on the inner mounting pads. The lead jacket is sealed around the teflon and lead mounting pads with a flexible epoxy resin. All critical seal areas then are covered with a layer of flexible silicone rubber caulk.

A typical encapsulated sample assembly is shown in Fig. 5. The jacketed sample with end caps comprises the lower two-thirds of the assembly, while the load cell and vessel closure make up the remainder. The vertical posts serve to position the sample on the load cell, while the spiral tube and one similar to it (not shown) connect the end caps to the vessel closure and, ultimately, to the pore pressure reservoirs. The conductance electrode leads exit the jacket at the top end cap and are connected to the electrical feed throughs at the vessel closure. The acoustic and strain gauge transducers can be seen near the middle of the sample.

Fractured samples are prepared by inducing a throughgoing tensile crack parallel to the sample axis by the Brazil method. The sample is then jacketed as described above, except for 0.1-mm Mylar and 0.2-mm stainless-steel shims which are centered over the crack and placed between the inner and outer tape layers. These shims prevent the lead jacket from extruding into the crack and rupturing. All transducers are located such that conductance, velocity, amplitude, and strain measurements are performed nearly parallel and perpendicular to the crack.

III. APPARATUS

All measurements are accomplished in a pressure vessel with the vessel walls serving as a reaction frame (see Fig. 6). Deviatoric stresses are determined from the sample cross-sectional area and an axial load cell in series with the sample. Loads on the sample may be applied with the moveable piston. Pore fluid and electrical feed throughs are located in the top vessel closure and retaining nut. The vessel is capable of confining pressures to 200 MPa and deviatoric stresses to 500–800 MPa (depending on confining pressure).

An LSI-11 microcomputer is used to control the confining pressure and deviatoric stress to 0.01 and 0.05 MPa, respectively. The confining pressure and axial load pressure system is shown schematically in Fig. 7. The computer control system will be discussed in detail later.

The pore fluid system used for low permeability measurements ($<10^{-17}$ m^2) is shown schematically in Fig. 8.

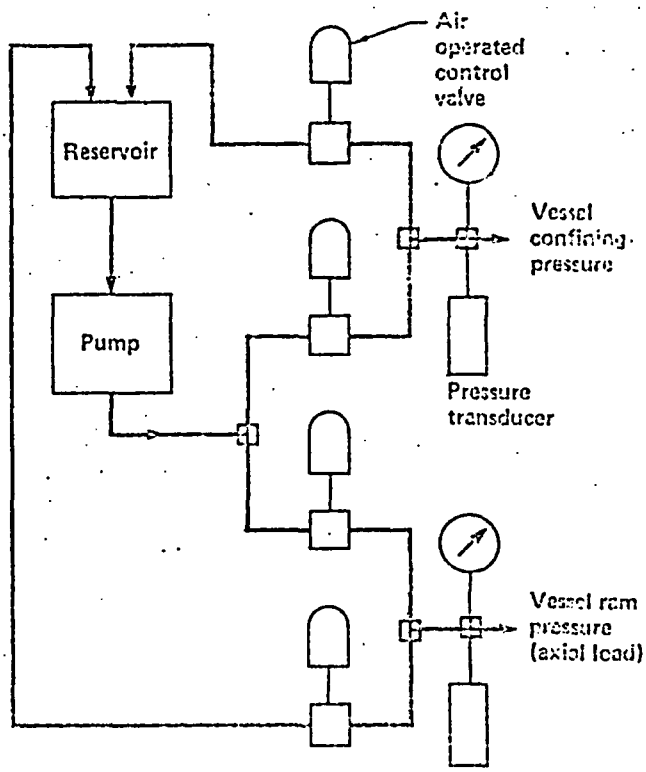

FIG. 7. Schematic of the pressure system for confining pressure and axial load.

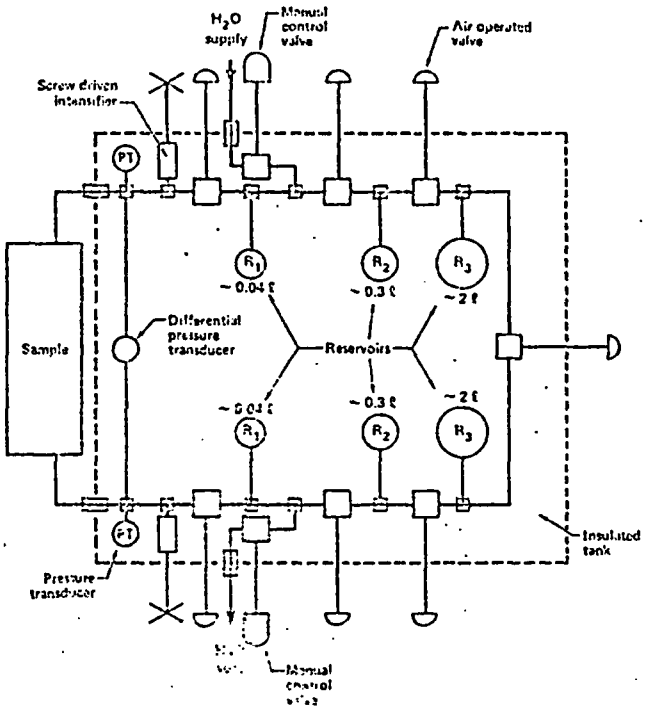

FIG. 8. Schematic of the pore pressure system for low-permeability ($<10^{-17}$ m²) measurements. The components shown inside the dashed rectangle are located in an insulated enclosure for thermal stability.

the diurnal temperature variation of 2°–3 °C are reduced to 0.1 °C by enclosing in an insulated tank as much of the plumbing system as possible, thereby reducing pressure fluctuation during the test. The tank is insulated with 0.1 m of polyurethane foam. Use of the insulated tank reduced the pressure fluctuations associated with the diurnal temperature variations from 0.6 to 0.02 MPa. The lower limit for permeability determinations was subsequently reduced from 10^{-22} to 10^{-24} m². The tank is so designed that it may be filled with water if more thermal stability is required.

During the course of a permeability measurement, changes in the reservoir pressures are monitored by two absolute pressure transducers to ±0.01 MPa and a differential pressure transducer to ±0.001 MPa. The volume of water (ΔV) entering or leaving a reservoir for a given change in pressure (ΔP) is

$$\Delta V = \Delta P \beta V_0 + \Delta P \gamma V_0 ,$$

where β is the compressibility of water, V_0 is the reservoir volume, and γ is the compliance of the reservoir and plumbing system.

The system compliance was evaluated by using a screw-driven intensifier to induce a known volume change in the reservoir. The resulting change in pressure was monitored with the pressure transducers. The results indicated that the system compliance was not negligible compared to the compressibility of water. Therefore, the effective reservoir volume V_e was defined as

$$V_e = V_0\left(1 + \frac{\gamma}{\beta}\right)$$

and

$$\Delta V = \Delta P \beta V_e .$$

The empirically determined effective reservoir volumes are used as the reservoir volumes for all permeability determinations. Forster and Gale[8] also noted the importance of system compliance by using a similar technique for field measurements; however, they chose to account for this effect by modifying the boundary conditions rather than by defining an effective volume.

Effective reservoir volumes of 0.005, 0.04, 0.34, and 2.4 l may be selected depending upon the sample permeability (see Fig. 8). The screw-driven intensifier may be used to increase these effective volumes up to 0.011 l with infinite resolution. The screw-driven intensifier is also used to evaluate effective volumes and to induce the step increase in pressure at the beginning of a measurement.

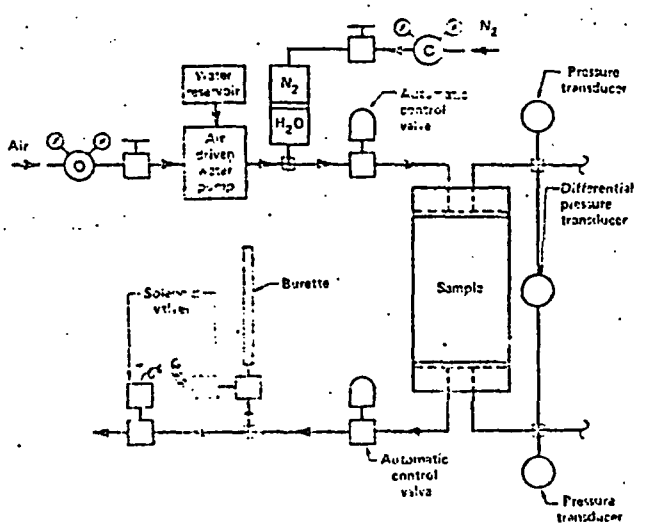

FIG. 9. Schematic of the pore pressure system for high permeability ($>10^{-17}$ m²) measurements. The pressure transducers are also used for the low permeability measurements (see Fig. 8).

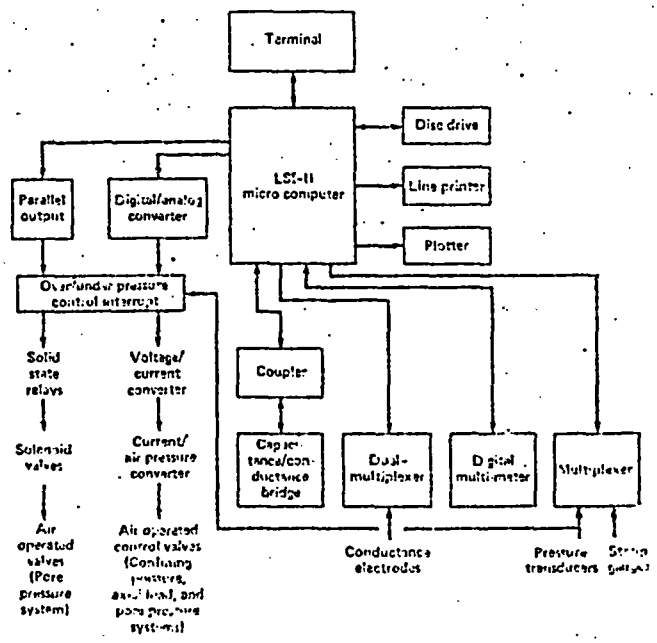

FIG. 10. Schematic of the experimental control and data-acquisition and reduction system.

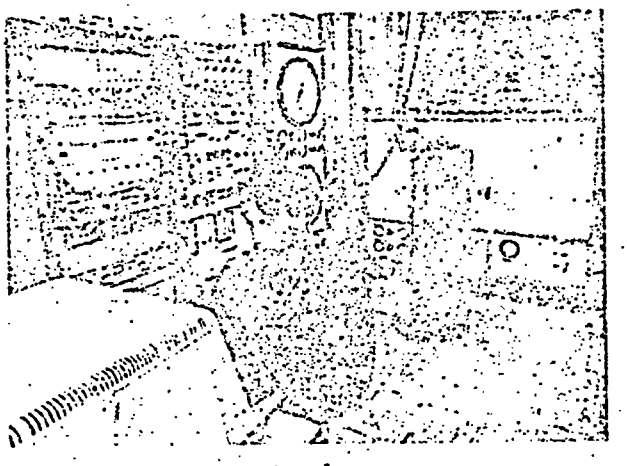

FIG. 11. Complete permeability apparatus. The pressure vessel and pore pressure system are to the right. The confining and axial load pressure system and the instrumentation rack are on the left. The terminal is in the foreground. The acoustic velocity, amplitude instrumentation, and the plotter are not shown.

The system for high-permeability (10^{-17}–10^{-11} m^2) determinations is shown schematically in Fig. 9. A permeability determination is performed by establishing a pressure drop across the sample and monitoring the resulting volume flow rate. The pressure is held constant with the control valves. A separator with pore fluid on one side and gas on the other is used to damp the pressure pulses from the water pump. The flow rate through the sample is monitored with a burette and a stop watch. The absolute pore pressure and the pressure drop across the sample are monitored with the pressure transducers described above. These pressure transducers are connected to the high permeability measurement system through grooves in the sample end caps at the end-cap/sample interface; therefore, the flow-induced pressure drops in the tubing may be ignored. The pressure drops established across the sample are typically 0.01–0.2 MPa. The permeability is evaluated at several different pressure drops to verify that the measurements were performed in the Darcy flow regime.

For rocks possessing very low permeabilities, a permeability determination may last 10^6 s or more; therefore, a means for automatic experimental control and data acquisition is desired. Experimental control and data acquisition is performed by an LSI-11 microcomputer system (see Fig. 10). To operate the control valves, digital signals from the microcomputer are converted to air pressure signals. The experiment is protected with an analog device which interrupts the control signals during a power failure or when pressures violate over/under pressure set points. Pressure transducer and strain gauge signals are monitored with a multiplexer and a digital multimeter to 0.001% or 1 μV. The conductances are monitored with a dual multiplexer and an automated capacitance/conductance bridge. The conductance across any two sample electrodes may be monitored. Conductivities of 10^{-3} to 10^{-9} Ω^{-1} may be measured with an accuracy of 0.1% to 10%, depending on the capacitance and conductance of the sample. The acoustic velocity and amplitude measuring system is described in Trimmer *et al.*[3] All pressure, strain, and conductance data are stored on disc.

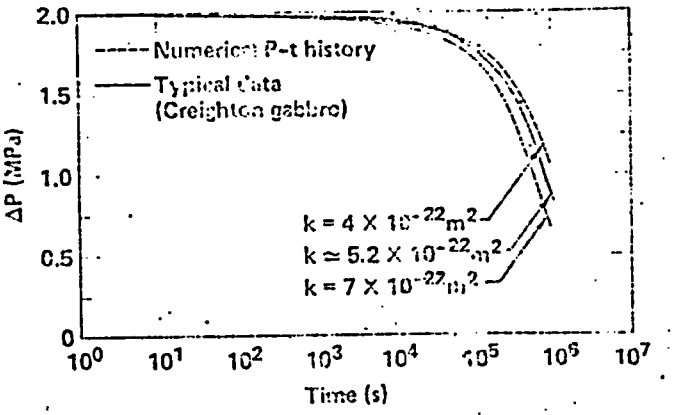

FIG. 12. Typical pressure decay curve for a very low-permeability material (>10^{-22} m^2). The sample was intact.

The current experimental data and the data acquisition and control parameters are displayed on the graphics terminal. Experimental control and data-acquisition parameters may be modified during an experiment. All data reduction, including the generation of numerical pressure–time histories, is performed on the microcomputer. The plotter is used for visually matching experimental data with the numerical pressure–time histories as indicated in Fig. 3. The experimental apparatus and instrumentation system is pictured in Fig. 11.

IV. TYPICAL RESULTS

For samples with permeabilities of 10^{-22} to 10^{-11} m^2, the permeability can be determined with an [illegible] 5% to 10%. For lower permeabilities, the [illegible] to 40% depending on how much of the pressure decay curve is produced within the time allocated for [illegible]. Longer tests would obviously yield higher accuracies. A

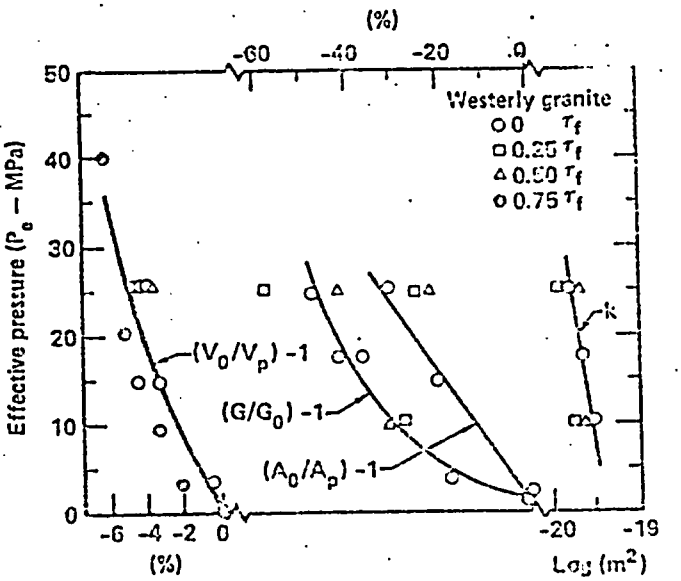

FIG. 13. Permeability, acoustic velocity, pulse amplitude, and electrical conductance data for intact Westerly granite. Data from Nur and Simmons shown as solid circles.[10]

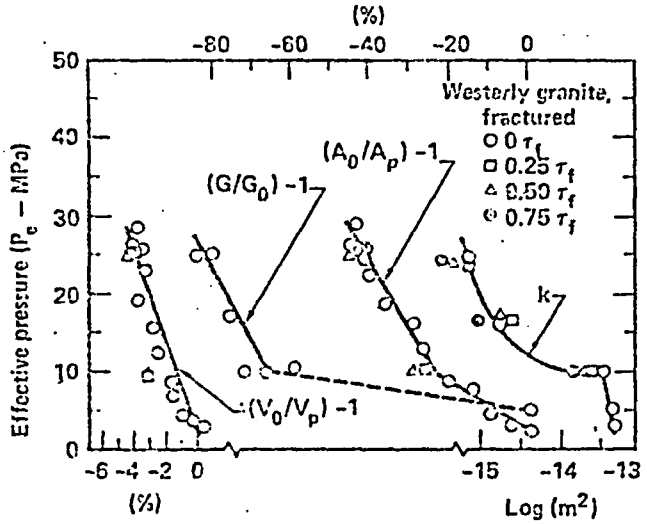

FIG. 14. Permeability, acoustic velocity, pulse amplitude, and electrical conductivity data for fractured Westerly granite.

typical pressure decay curve for a sample having a permeability of $\sim 10^{-20}$ m² is shown in Fig. 3(b). A typical pressure decay curve for a lower permeability sample ($\sim 10^{-22}$ m²) is shown in Fig. 12.

Figure 13 shows permeability data as well as normalized conductance, acoustic velocity, and amplitude data for Westerly granite. The acoustic velocity, amplitude, and conductance data exhibit a good correspondence with the permeability data. However, the velocity data is of less interest since the relative changes are small. Figure 14 shows the same type of data for fractured Westerly granite. As in the case of the intact rock, the acoustic and conductance data show a good correspondence with the permeability data. We believe that the inflection points at 10 MPa for the conductance, acoustic amplitude, and permeability reflect a transition from the crushing of the asperities and included grains in the fracture to the quasielastic closing of the fracture at higher pressures.

Changes in crack apertures for fractured samples were monitored with the strain gauge beam as noted above. Absolute fracture widths were estimated by plotting permeability versus the change in fracture width and by extrapolating the curve to complete closure. [illegible] width was considered to be zero at zero pressure. Typical results are shown in Fig. 15.

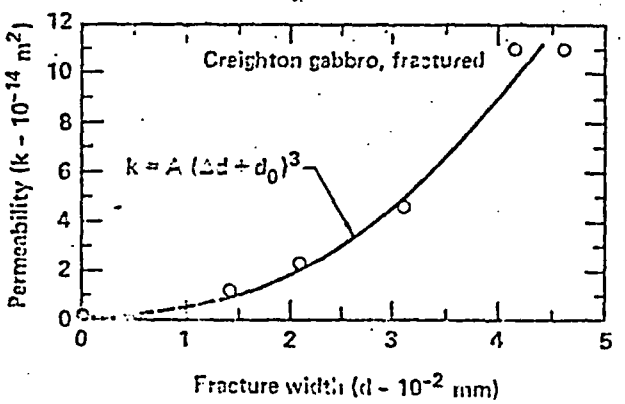

FIG. 15. Permeability vs fracture width for fractured Greighton gabbro.

APPENDIX A

The pulse technique for measuring permeability [illegible] modeled with a finite element computer code. [illegible] A-1 is a schematic of the sample-reservoir system. [illegible] sample is divided into n zones, with the reservoirs [illegible] the 0th and $(n+1)^{th}$ zones. The flow across each [illegible] interface is assumed to be constant for some time increment Δt. The flow across each zone interface is [illegible]

$$v_{i,i+1} = \frac{kA(P_{i+1} - P_i)}{\mu L_z}\Delta t, \quad i = 1, \ldots, n-1,$$

$$= \frac{kA(P_{i+1} - P_i)}{\mu(0.5L_z)}\Delta t, \quad i = 0 \text{ and } n,$$

where $v_{i,i+1}$ is the volume flow across the ith, [illegible] interface, P_i is the pressure in the ith zone, and L_z [illegible] zone length. The shorter zone length used for the 1st and n^{th} to $(n+1)^{th}$ interfaces reflects the [illegible] from the reservoirs to the middle of the adjacent [illegible] zones.

The new pore pressure distribution is then determined from the net fluid storage in each zone:

$$P_{i(t=t+\Delta t)} = P_{i(t=t)} + \frac{v_{i+1,i} - v_{i,i-1}}{AL_z\phi_e\beta}, \quad i = 1, n,$$

$$= P_{i(t=t)} - \frac{v_i}{v_{1e}\beta}, \quad i = 0,$$

$$= P_{i(t=t)} + \frac{v_i}{v_{2e}\beta}, \quad i = n+1,$$

where v_{1e} and v_{2e} are the upstream and downstream effective reservoir volumes, respectively. The new pore pressure distribution is then used in Eq. (A-1) to determine the flow for the next time increment, and so forth.

Inputs to the code are sample geometry, effective reservoir volumes (V_e), effective porosity (ϕ_e), the number of zones, sample permeability, and the time increment. The code has been checked for appropriate zone and time increments and for accuracy against the [illegible] code[9] and against analytical solutions.[4] This code agrees with the TRUMP code and the analytic solutions to [illegible] than 0.1%.

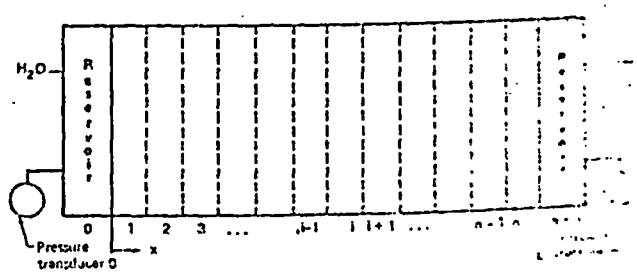

FIG. A-1. Model of the sample-reservoir system used in the [illegible] ment code.

ACKNOWLEDGMENTS

The author would like to thank the following individuals for the valuable advice and assistance given during the design, construction, and testing of this apparatus: G. Armstrong, E. Arnold, B. Bonner, C. Boro, A. Duba, H. Heard, and K. Keller.

This work has been supported by the National Waste Terminal Storage Program of the U.S. Department of Energy and was performed under the auspices of the U.S. Department of Energy by the Lawrence Livermore National Laboratory under contract number W-7405-ENG-48.

[1] W. F. Brace, J. B. Walsh, and W. J. Frangos, J. Geophys. Res. 73, 225 (1966).
[2] D. A. Trimmer, Geophys. Res. Lett. 8, 973 (1981).
[3] D. A. Trimmer, B. Bonner, H. C. Heard, and A. Duba, J. Geophys. Res. 85, 7059 (19[illegible]).
[4] P. A. Hsieh, J. V. Tracy, C. [illegible]ovail, J. D. Bredehoeft, and S. E. Silliman, Int. J. Rock Mech. [illegible] Sci. 18, 245 (1981).
[5] B. P. Bonner and R. N. Schock, [illegible]ic Velocities, *Physical Properties of Rocks and Min[illegible]*, edited by Y. S. Touloukian, C. Y. Ho, and W. R. Judd (McGraw-Hill, New York, 1980).
[6] R. J. Lytle, A. G. Duba, and J. L. Williams, Rev. Sci. Instrum. 50, 611 (1979).
[7] K. T. Keller, *Curved Beam Usage in the Remote Measurement of Radial Strains in Water Transport Samples*, Lawrence Livermore National Laboratory, Livermore, CA, UCRL re[illegible] (in preparation).
[8] C. B. Forster and J. F. Gale, *A Laboratory Assess[illegible] of the Use of Borehole Pressure Transients to Measure the Per[illegible]bility of Fractured Rock Masses*, Lawrence Berkeley Laboratory, Berkeley, CA, LBL-8674, SAC-23, UC-70, 1980.
[9] A. L. Edwards, *TRUMP: A Computer Program for Transient and Steady-State Temperature Distributions in Multidimensional Systems*, Lawrence Livermore National Laboratory, Livermore, CA, UCRL-14754, 1972.
[10] A. Nur and G. Simmons, Earth Planet. Sci. Lett. 7, 183 (1969).